



OPEN ACCESS

EDITED BY

Penelope Anne Morel,
University of Pittsburgh, United States

REVIEWED BY

Nahum Puebla-Osorio,
University of Texas MD Anderson Cancer
Center, United States
Haigang Wu,
Henan University, China

*CORRESPONDENCE

Magdalena Szafrńska-Łęczycka
✉ m.szafranska6@uw.edu.pl

[†]These authors have contributed
equally to this work and share
senior authorship

RECEIVED 20 January 2025

ACCEPTED 26 May 2025

PUBLISHED 18 June 2025

CITATION

Szafrńska-Łęczycka M, Szymańska Z,
Piotrowska MJ, Bodnar M and Foryś U (2025)
CAR-T cell therapy for glioblastoma:
insight from mathematical modeling.
Front. Immunol. 16:1563829.
doi: 10.3389/fimmu.2025.1563829

COPYRIGHT

© 2025 Szafrńska-Łęczycka, Szymańska,
Piotrowska, Bodnar and Foryś. This is an open-
access article distributed under the terms of
the [Creative Commons Attribution License
\(CC BY\)](https://creativecommons.org/licenses/by/4.0/). The use, distribution or reproduction
in other forums is permitted, provided the
original author(s) and the copyright owner(s)
are credited and that the original publication
in this journal is cited, in accordance with
accepted academic practice. No use,
distribution or reproduction is permitted
which does not comply with these terms.

CAR-T cell therapy for glioblastoma: insight from mathematical modeling

Magdalena Szafrńska-Łęczycka^{1*}, Zuzanna Szymańska²,
Monika J. Piotrowska^{3†}, Marek Bodnar^{3†} and Urszula Foryś³

¹Doctoral School of Exact and Natural Sciences, University of Warsaw, Warsaw, Poland,

²Interdisciplinary Centre for Mathematical and Computational Modelling, University of Warsaw, Warsaw, Poland, ³Institute of Applied Mathematics and Mechanics, Faculty of Mathematics, Informatics and Mechanics, University of Warsaw, Warsaw, Poland

Introduction: Glioblastoma is a rare, aggressive brain tumor marked by high therapeutic resistance, poor prognosis, and limited treatment options. Emerging immunotherapies, particularly Chimeric Antigen Receptor (CAR) T-cell therapy, offer promising alternatives to standard care. However, adapting CAR-T cell strategies from hematologic malignancies to solid tumors like glioblastoma presents substantial challenges.

Methods: We extended existing mathematical models to investigate glioblastoma treatment dynamics with CAR-T cell therapy. Simulations were based on clinical trial-inspired scenarios targeting IL13R α 2, HER2, and EGFRvIII antigens, assessing both single-dose and cyclic dosing regimens. The models incorporated key biological processes, including tumor growth, CAR-T cell proliferation delays, and resistance mechanisms.

Results: Cyclic CAR-T cell administration outperformed single-dose strategies in reducing tumor burden. Incorporating resistance and treatment delays into the models provided critical insights into relapse dynamics and therapeutic durability.

Discussion: This study presents a comprehensive modeling framework for CAR-T cell therapy in glioblastoma, highlighting the importance of dosing regimens and resistance dynamics. The findings offer valuable guidance for optimizing therapeutic strategies to enhance patient outcomes.

KEYWORDS

CAR-T cell therapy, glioblastoma, cyclic treatment, single-dose strategies, mathematical modeling, numerical simulations

1 Introduction

Glioblastoma is a rare, highly aggressive brain tumor characterized by therapeutic resistance and poor survival outcomes in both adults and children. Despite advancements in brain cancer research, translating insights into glioblastoma pathogenesis into improved clinical outcomes remains a critical unmet need Wu et al. (1) Dewdney et al. (2). The standard treatment for glioblastoma includes surgical resection followed by chemoradiotherapy Wu et al. (1) Migliorini et al. (3). However, robust DNA repair mechanisms and the self-renewing capacity of glioblastoma cells drive resistance to existing therapies, resulting in a 5-year survival rate of only 7.2% Wu et al. (1). Achieving durable glioblastoma management requires novel strategies, with research focusing on targeted molecular inhibitors, nanoparticle delivery systems, and immunotherapies Wu et al. (1).

Among immunotherapies, cellular approaches such as chimeric antigen receptor (CAR)-T cell therapy hold significant promise for treating brain tumors Dewdney et al. (2). Research on CAR-T cells began in the late 20th century Eshhar et al. (4), focusing on harnessing the immune system to combat cancer. In this therapy, a patient's T cells are collected via apheresis and genetically modified *ex vivo* to express a chimeric antigen receptor (CAR) Dewdney et al. (2). The chimeric antigen receptor enables T cells to specifically recognize and eliminate tumor cells. After genetic engineering, the T cells are multiplied and reintroduced into the patient. In a clinical trial by Wrona and Potemski (5), 50.5% of patients with hematologic cancers survived at least two years after CAR-T therapy. This approach has also shown efficacy against colorectal cancer, breast cancer, and pancreatic ductal adenocarcinoma Kufel and Lewandowski (6). Current studies report BCMA-specific CAR-T cells achieving therapeutic responses in 20–64% of patients with relapsed or refractory multiple myeloma Cohen et al. (7). CAR-T therapy has recently been employed to treat B-cell acute lymphoblastic leukemia Pasvolsky et al. (8), with CD19-targeted CAR-T cells inducing complete remission in nearly 90% of patients with relapsed or refractory cases – significantly outperforming the less than 45% remission rate of conventional chemotherapy Park et al. (9).

Building on the success of CAR-T cell therapies in treating cancers, especially hematological ones, researchers are now working to extend these advances to aggressive solid tumors like glioblastoma. To aid this effort, mathematical models are being developed to better understand disease dynamics and treatment strategies. León-Triana et al. (10) proposed a four-dimensional mathematical model using differential equations to describe CAR-T cell therapy for glioma. The model incorporates two CAR-T cell populations (inside and outside the tumor), tumor cells, and B cells in dual-target treatment. It assumes exponential tumor growth and simulates a single CAR-T cell dose at treatment onset. Results suggest that single-target CAR-T cells require unrealistically high doses to overcome immune suppression, while dual-target CAR-T cells enable effective expansion and sustained tumor control. This approach holds promise for glioblastoma treatment, particularly when applied immediately after surgical resection and before cytotoxic therapy.

The model by León-Triana et al. (10) was later modified to explore CAR-T cell–tumor interactions under different treatment protocols. Bodnar et al. (11) introduced a two dimensional model focusing on CAR-T and tumor cell dynamics. While assuming exponential tumor growth, they analyzed multiple treatment scenarios, including continuous and intermittent CAR-T cell administration. Their results suggest that cyclic or continuous dosing is more effective than a single-dose strategy. A similar conclusion was reached in Bodnar et al. (12), which examined a modified four-dimensional model based on León-Triana et al. (10). This study incorporated logistic tumor growth and varied treatment regimens, highlighting that administering the highest possible dose at regular intervals outperforms a continuous moderate dose. Furthermore, intermittent dosing effectively extends tumor control, even with a lower average dose. Recently, Szafrńska-Lęczycska et al. (13) proposed a two-variable model, similar to Bodnar et al. (11, 12), but with a time delay to account for mitosis duration in cancer cell proliferation. This study focused on single-dose administration, enabling rigorous analysis of its effects. Results showed that complete tumor elimination was unachievable regardless of dose size, raising concerns about the long-term efficacy of single-dose treatments.

1.1 Clinical CAR-T approaches to glioblastoma treatment

Migliorini et al. (3) reported the results of three first-in-human CAR-T cell trials targeting IL13R α 2, Her2/CMV, and EGFRvIII. We refer to these CAR-T cell therapy scenarios as the first, second, and third approaches to treatment, terms that are used consistently throughout the paper. The target antigen in the first approach to treatment was the IL13R α 2 receptor. In this method, CAR-T cells were initially administered directly into the resection cavity using a Rickham catheter and subsequently into the brain's ventricle. These CAR-T cells featured a mutated IL-13 domain (IL13 E13Y) in the antigen-binding site. Although significant tumor regression was observed following intraventricular administration, recurrence occurred later due to the loss of the IL13R α 2 antigen. The second approach to the treatment targeted the HER2 receptor. CAR-T cells in this method were engineered to include the FRP5 (anti-HER2 scFv) domain, CD28 (for co-stimulation), and CD3 ζ (for signal activation). The cells were administered intravenously at intervals of 6–12 weeks, with a maximum of seven cycles. These CAR-T cells remained in the body for up to 12 months, albeit in low numbers. One patient demonstrated a significant radiological response, while five patients experienced disease stabilization for over 24 months. The third approach to treatment involved a single infusion of CAR-T cells engineered with a humanized scFv domain targeting EGFRvIII, along with 4-1BB (for co-stimulation) and CD3 ζ (for signal activation). These cells exhibited peak activity between days 3 and 10 but were undetectable after 30 days. Notably, one patient achieved disease stabilization lasting over 18 months. Comparing these approaches, the second method appears to be the safest, with doses ranging from 1×10^6 to 1×10^8 cells/m² of patient body

Migliorini et al. (3). This treatment regimen aligns with findings from Scharovsky et al. (14), which suggest that cyclic drug administration at regular intervals – typically in small doses with minimal rest periods – is the most effective strategy for cancer treatment. Indeed, administering the maximum tolerated dose in conventional therapies necessitates rest periods between treatment cycles, which can allow cancer to regrow and promote the emergence of therapy-resistant clones.

1.2 Research goals

Building on previous mathematical models, we aim to provide deeper insights into disease dynamics under CAR-T cell treatment. To achieve this, we modify earlier mathematical modeling attempts to reflect the treatment regimens described by Migliorini et al. (3). In the first approach, this involves incorporating a mathematical description of emerging resistance to treatment. The second and third approaches to treatment involve introducing a delay to account for the time required to activate CAR-T cells at the tumor site. We further present a comparison of the three approaches, which not only facilitates the identification of the most effective treatment strategies but also deepens our understanding of the factors influencing relapse or patient recovery. This comprehensive analysis provides valuable insights that can guide the optimization of CAR-T cell therapy protocols and improve patient outcomes.

Therefore, in this paper, our first goal is to reflect three CAR-T therapy scenarios studied in Migliorini et al. (3) using two simple modifications of mechanistic models proposed and analyzed in León-Triana et al. (10)–Szafrńska-Łęczyccka et al. (13). In line with the treatment approaches Migliorini et al. (3), we consider a single-dose treatment strategy and cyclic CAR-T administration. We analyze the significance of the resistance to the therapy as well as the immune system's response time to the administered CAR-T cells in the considered treatment strategies. Furthermore, we evaluate the potential benefits of cyclic CAR-T cell administration compared to a single-injection approach, and investigate the dose of CAR-T cells and the distance between subsequent doses required to achieve the best treatment outcomes. We perform sensitivity analysis, to find the models parameters most influential to the model's dynamics. Naturally, the effects of treatment may vary depending on tumor size, the method of administration, and the administered dose of CAR-T cells. In the worst-case scenario, the tumor may grow to its maximum size while the CAR-T cell population diminishes entirely. Basing on our models suggestions we propose treatment strategies allowing for elongation of time to progression.

2 Materials and methods

2.1 Models

Let us begin by considering a basic model, which is a modified version of the one proposed by León-Triana et al. (10). It consists of two differential equations describing the temporal dynamics of

glioma cells $T(t)$ and CAR-T cells $C(t)$). In the original model by León-Triana et al. (10), the authors assumed unlimited tumor growth. Considering this an oversimplification, we instead model tumor growth as constrained by the environment's carrying capacity, using a logistic growth term. Note that this type of growth has a simple mathematical form. Yet, it can be considered representative of the variety of growth functions found in the literature [cf. the discussion on the biological background in Bodnar and Foryś (15)]. Here, we adopt a specific form of growth due to the quantitative nature of our analysis. However, from a mathematical perspective, qualitative results can often be obtained by making general assumptions about the growth function, as in previous work Bodnar et al. (12). Recognizing the importance of calibrating biological models, we are pursuing research in this direction, while acknowledging that it remains a complex task – even for simplified models Szymańska et al. (16) Gwiazda et al. (17).

Additionally, CAR-T cells actively eliminate tumor cells, a process represented by a bi-linear interaction term. The dynamics of CAR-T cells also account for their proliferation rate, inactivation, and natural death. The model, partially analyzed in Bodnar et al. (11, 12) and then in Szafrńska-Łęczyccka et al. (13), is described by the following system:

$$\begin{aligned} \frac{d}{dt} T(t) &= \rho_T T(t) \left(1 - \frac{T(t)}{K}\right) - \alpha_T C(t) T(t), \\ \frac{d}{dt} C(t) &= \left(\frac{\rho_C T(t)}{g_T + T(t)} - \frac{\alpha_C T(t)}{g_C + C(t)} - \frac{1}{\tau_C} \right) C(t), \end{aligned} \quad (1)$$

where all parameters are assumed to be positive. The parameter ρ_T represents the tumor growth rate, defined as the difference between the proliferation rate and the natural cell death rate. The term $\rho_T T \left(1 - \frac{T}{K}\right)$ describes the development of a tumor in conditions of lack of immune system activity. The assumed logistic growth implies that the tumor's expansion is limited, with K representing the tumor's carrying capacity, or in other words, the maximum possible tumor size. We assumed that CAR-T cells eliminate cancer cells with an efficiency described by the parameter α_T . The CAR-T cell dynamics equation includes three key processes. The first term describes CAR-T cell proliferation, which is triggered by contact with tumor cells and occurs at a maximum rate ρ_C . Note that this process is saturated, meaning that it is proportional to the tumor size only for small tumors, while for larger tumors it tends to the constant value ρ_C . Half saturation level g_T reflects the tumor size for which proliferation reaches a half of maximal value ρ_C . The second term models CAR-T cell inactivation by tumor cells at a maximum rate α_C , with a half-saturation level g_C . This inactivation reflects mechanisms such as CAR-T cell dysfunction induced by the tumor microenvironment. Finally, the third term accounts for the natural death or inactivation of CAR-T cells, with their average lifespan denoted by τ_C .

Note that in the model Equation 1, we included only the most essential aspects of the considered therapy to maintain analytical tractability and minimize the number of parameters. The model does not account for key factors such as drug resistance or delayed immune response, which are crucial for accurately modeling the clinical trials discussed in Migliorini et al. (3). Therefore, the model would need to be adjusted accordingly.

The first approach to glioma treatment with CAR-T cell administration involved direct delivery through a Rickham catheter into the brain’s ventricle as described by Migliorini et al. (3). The treatment regimen began with the administration of an initial dose followed by additional administrations of CAR-T cells, again delivered via a Rickham catheter, at weekly intervals with the break before the last cycle, for detail description of the protocol see Subsection 2.2.3.

This method, although very promising at first, was associated with the rapid development of drug resistance. The precise mechanisms of this drug resistance remain unknown, but more information is available regarding its dynamics, thus we modeled it by introducing a time-dependent variable ($R(t)$). Hence, to model the first approach to treatment, we included an additional equation in the basic model, given by Equation 1, describing the strength of drug resistance:

$$\begin{aligned} \frac{d}{dt} T(t) &= \rho_T T(t) \left(1 - \frac{T(t)}{K}\right) - \alpha_T (1 - R(t)) C(t) T(t), \\ \frac{d}{dt} C(t) &= \left(\frac{\rho_C (1 - R(t)) T(t)}{g_T + T(t)} - \frac{\alpha_C T(t)}{g_C + C(t)} - \frac{1}{\tau_C} \right) C(t), \\ \frac{d}{dt} R(t) &= \alpha_R C(t) (1 - R(t)). \end{aligned} \tag{2}$$

Drug resistance is modeled as reducing α_T and ρ_C , indicating that greater resistance leads to lower treatment efficacy and weaker CAR-T cell proliferation. The factor $1 - R(t)$, which scales α_T and ρ_C in the first and second equations, respectively, represents this diminishing efficacy. Resistance changes over time proportionally to the CAR-T cell population, with self-inhibition preventing unlimited growth. A similar approach to modeling drug resistance was previously employed in Elishmereni et al. (18) Forýs et al. (19).

We follow this idea and therefore maintain a simple, minimally parameterized model, as noted earlier.

In the second and third approaches to glioma treatment described by Migliorini et al. (3), involving cyclic and single intravenous administration of CAR-T cells, respectively, drug resistance is negligible and excluded from the model. However, since CAR-T cells were administered intravenously, they required time to cross the blood-brain barrier and migrate to the tumor site. To address this, we introduced a time delay, τ (in days), representing the duration needed for CAR-T cells to reach the tumor, activate, and proliferate after interacting with cancer cells. Thus, the increase in activated CAR-T cells depends on the earlier states of $T(t)$ and $C(t)$ at time $t - \tau$, leading to the following model

$$\begin{aligned} \frac{d}{dt} T(t) &= \rho_T T(t) \left(1 - \frac{T(t)}{K}\right) - \alpha_T C(t) T(t), \\ \frac{d}{dt} C(t) &= \rho_C \frac{T(t-\tau) C(t-\tau)}{g_T + T(t-\tau)} - \left(\frac{\alpha_C T(t)}{g_C + C(t)} + \frac{1}{\tau_C} \right) C(t). \end{aligned} \tag{3}$$

The model, in this form has been mathematically analyzed by Szafrańska-Łęczycska et al. (13). It is worth noting that introducing a delay into the model may result in oscillatory behavior of the solutions. While such oscillations can occasionally be observed in medical treatments, they are generally undesirable in therapy and they can interfere with the oscillations caused by the cyclic administration of CAR-T cells.

2.2 Numerical simulation setup

2.2.1 Parameters

All model parameters and their reference values are defined as positive constants and are summarized in Table 1. Note that the parameter α_R appears only in model Equation 2. Although the presented models include eight main parameters, however, for model Equation 3 the delay τ is also treated as an additional parameter.

TABLE 1 Parameters of models Equations 2 and 3 together with the initial conditions defined by Equation 4: reference values, ranges and corresponding references.

Name	Description	Ref. value	Range	Units	Reference
ρ_T	tumor growth rate	0.01	$\pm 20\%$	day ⁻¹	Stein et al. (20)
K	maximum tumor size	2×10^{12}	$\pm 20\%$	cell	estimated
α_T	inactivation of CAR-T cells by tumor	2.5×10^{-10}	$\pm 20\%$	day ⁻¹ cell ⁻¹	León-Triana et al. (10)
ρ_C	CAR-T proliferation	0.9	$\pm 20\%$	day ⁻¹	Stein et al. (20)
g_T	tumor half-saturation level	1×10^{10}	$\pm 20\%$	cell	Stein et al. (20)
α_C	CAR-T inactivation rate	0.05	$\pm 20\%$	day ⁻¹	Radunskaya et al. (21)
g_C	CAR-T half-saturation level	2×10^9	$\pm 20\%$	cell	Radunskaya et al. (21)
τ_C	active CAR-T cell mean lifetime in the tumor site	7	$\pm 20\%$	day	Ghorashian et al. (22)
α_R	drug resistance factor	8×10^{-10}	$\pm 20\%$	day ⁻¹	estimated
τ	mean time needed to trigger the production of CAR-T cells in the organism	2	$\pm 20\%$	day	Qi et al. (23)
T_0	initial average number of tumor cells	1.5×10^{10}	$\pm 20\%$	cell	estimated
C_0	initial average number of CAR-T cells	2×10^7 (★) 5×10^8 (★★)	$\pm 20\%$	cell	Migliorini et al. (3) Bodnar et al. (12)
R_0	initial cancer cell resistance	0	—	—	estimated

(★) value used to perform the sensitivity analysis for model Equation 2, (★★) value used to perform the sensitivity analysis for model Equation 3.

2.2.2 Initial conditions

To run simulations for considered models the initial conditions need to be defined. In the case of Equation 1, this means specifying the values of $T(0)$ and $C(0)$, which we assume to be:

$$T(0) = T_0 > 0 \quad \text{and} \quad C(0) = C_0 > 0. \quad (4)$$

In the case of Equation 2, the model is extended by an equation describing acquired drug resistance. This equation also requires an initial condition to be defined at the beginning of the simulation, leading to the following initial condition:

$$T(0) = T_0 > 0 \quad \text{and} \quad C(0) = C_0 > 0 \quad \text{and} \quad R(0) = R_0 = 0. \quad (5)$$

For delay differential equations, such as Equation 3, the initial conditions must be defined as a function on the interval $[-\tau, 0]$. In the absence of CAR-T cells, we assume that tumor growth follows a logistic pattern. Consequently, the initial condition for $T(t)$ is defined as:

$$T(t) = \frac{K}{1 - \left(1 - \frac{K}{T_0}\right)e^{-\rho\tau t}}, \quad \text{for } t \in [-\tau, 0]. \quad (6)$$

Since the effects of CAR-T therapy commence at $t = 0$, we assume $C(t) = 0$ for $t \in [-\tau, 0)$, with a dose C_0 administered at $t = 0$. These assumptions lead us to the following initial condition for $C(t)$

$$C(t) = \begin{cases} 0, & \text{for } t \in [-\tau, 0), \\ C_0 > 0, & \text{for } t = 0. \end{cases} \quad (7)$$

2.2.3 Treatment protocols

The third approach to treatment assumes a single dose of CAR-T cells administered at the beginning of treatment. Modeling this approach is relatively straightforward, as it requires setting an appropriate initial condition, where the initial value, C_0 , corresponds to the administered dose. The first and second approaches to treatment described by Migliorini et al. (3), involve multiple doses of CAR-T cells administered at predefined time intervals.

These approaches necessitate a different model formulation to account for the repeated dosing schedule. We present them in concise form in Table 2. To mimic time-staggered dosing within the treatment regimen we used impulses to represent cyclically administered doses given at times $t_n = nP$, where $n \in \mathbb{N}, n > 1$, and P is the time interval between two consecutive cell administrations, see Figure 1. This leads to impulsive equations, where Equations 2 and 3 are solved for $t \in [t_n, t_{n+1})$, with

$$T(t_n) = \lim_{t \rightarrow t_n^-} T(t), \quad C(t_n) = \lim_{t \rightarrow t_n^-} C(t) + m, \quad (t_n) = \lim_{t \rightarrow t_n^-} R(t)$$

for Equation 2, and

$$T(t_n) = \lim_{t \rightarrow t_n^-} T(t), \quad C(t_n) = \lim_{t \rightarrow t_n^-} C(t) + m$$

for Equation 3, where m denotes a single CAR-T cell dose administered at time $t = nP$.

To evaluate the first approach targeting the IL13R α 2 receptor, we used the model defined by Equation 2 with initial condition (5). The first approach to glioma treatment with CAR-T cell administration involved direct delivery through a Rickham catheter into the brain's ventricle as described by Migliorini et al. (3). The treatment regimen began with the administration of an initial dose of 2×10^6 cells. This was followed by 5 doses of 1×10^7 cells delivered via a Rickham catheter at weekly intervals, and an additional 10 doses of the same amount administered through a new Rickham catheter. After a 5-week break, the final 4 doses of 1×10^7 cells were administered, also at weekly intervals. The schematic diagram of the treatment scheme is shown in Figure 1A, while the corresponding values are summarized in the first row of Table 2.

To evaluate the second approach targeting the HER2 receptor, we simulated the model described by Equation 3 with initial conditions (6) and (7). The simulations involved cyclic administration of seven equal CAR-T cell doses (an initial dose followed by six additional doses) at intervals ranging from 6 to 12 weeks, based on the methodology of Migliorini et al. (3). This methodology specifies that each CAR-T cell dose ranges from 1×10^6 cells/m² to 1×10^8 cells/m². We assume a sample patient with a body weight of 70kg and a height of 180cm. Using the Haycock formula, we calculated the range of doses that could be administered at each time point for the patient, see Haycock et al. (24). Consequently, each dose consider in our analysis falls within the range of 1.89×10^6 to 1.89×10^8 cells. The schematic diagram of the treatment scheme is shown in Figure 1B, while the corresponding values are summarized in the second row of Table 2.

To evaluate the third approach to treatment targeting EGFRvIII, we once again used Equation 3 with initial conditions (6) and (7), set to represent a single dose of CAR-T cells of 5×10^8 cells administered at the start of the treatment. The schematic diagram of the treatment scheme is shown in Figure 1B, while the corresponding values are summarized in the third row of Table 2.

2.2.4 Effectiveness of treatment protocols

To conduct a systematic study of the effect of dose distribution (dose size and time between injections) for the first approach to treatment we used model Equation 2 with initial condition (5). According to Migliorini et al. (3) we kept the first dose unchanged (2×10^6 cells) while varied the size of subsequent doses and the time

TABLE 2 Summary of CAR-T cell treatment protocols targeting IL13R α 2, Her2/CMV, and EGFRvIII.

Target	Administration route	Number of doses	Dose size	Model
IL13R α 2	Intracranial (via Rickham catheter into the ventricle)	20	First dose: 2×10^6 Subsequent doses: 1×10^7	(2)
Her2/CMV	Intravenous	1–7	1.89×10^6 , 1.89×10^7 , or 1.89×10^8	(3)
EGFRvIII	Intravenous	1	5×10^8	(3)

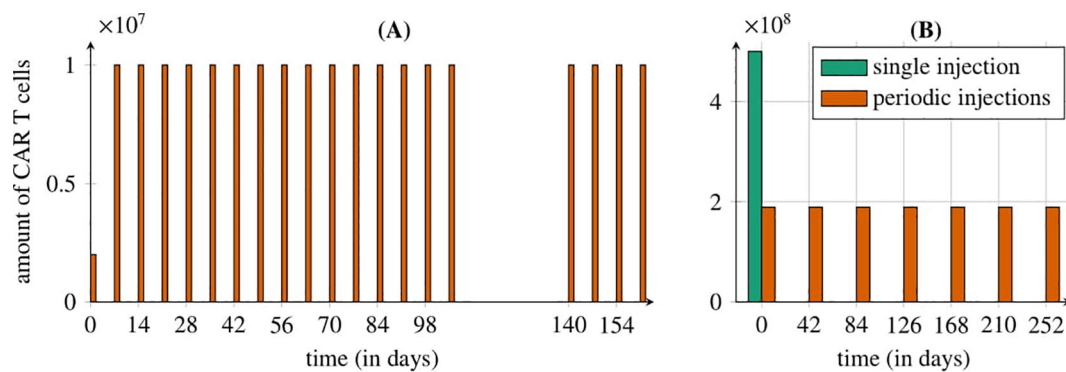


FIGURE 1

Representation of the treatment protocols studied by Migliorini et al. (3). (A) Cyclic injections of IL13R α 2 CAR-T cells directly into the resection cavity via a Rickham catheter (first approach): starting with an intracerebroventricular dose of 2×10^6 CAR-T cells, followed by 19 weekly cycles of 10×10^6 cells, with a 5-week break between the 15th and 16th doses. (B) Intravenous administration of CAR-T cells in two ways (second and third approaches): seven cyclic HER2/CMV CAR-T injections every six weeks (1.89×10^6 cells each, orange bars) or a single EGFRvIII CAR-T dose of 5×10^6 cells (green bar). The treatment is modeled for a 70 kg, 180 cm patient with a tumor of 1.5×10^{10} cells.

intervals between infusions, ensuring that the total administered amount of CAR-T cells maintain fixed (1.9×10^8 cells) and equivalent to 19 doses of 10^7 cells administered in the trial tested by Migliorini et al. (3).

A single dose size d_i was calculated as:

$$d_i = \frac{1.9 \times 10^8}{i}, \text{ for } i = 1, \dots, 19. \quad (8)$$

For all tested protocols we compared tumor cell population 540 days after treatment initiation.

For the second approach to treatment, we utilized the model described by Equation 3 with initial conditions (6) and (7). We analyzed the significance of dose size, the number of subsequent doses, and the time interval between injections, following the methodology outlined by Migliorini et al. (3). Specifically, we examined equal-dose protocols throughout the entire treatment (including the initial doses), with single dose sizes of 1.89×10^6 , 1.89×10^7 , and 1.89×10^8 cells, as detailed in Subsection 2.2.3. In other words, we focused on analyzing the effect of administering one to six additional doses, added to the initial dose, and the interval between them, on the treatment outcome. The impact of these treatment protocols on tumor cell population dynamics was evaluated 540 days after treatment initiation.

The efficacy of the third approach to treatment targeting EGFRvIII, modeled using Equation 3 with initial conditions (6) and (7), depended solely on a single dose of CAR-T cells administered at the start of treatment. Thus, it offered limited opportunities for manipulation or optimization.

To additionally evaluate the effectiveness of considered protocols we calculated time to progression (TTP) as it is a key measure for assessing treatment effectiveness in medicine. TTP is defined as the time (expressed in days) needed for the tumor to re-grow to the initial size i.e. to the size before the given treatment started.

2.2.5 Tools

Numerical simulations and sensitivity analyses are conducted using MATLAB's 4th-order Runge-Kutta method for Equation 2 and MATLAB's 2nd-order Runge-Kutta method for Equation 3; see The MathWorks Inc. (25).

2.2.6 Sensitivity analysis

Sensitivity analysis is a method used to evaluate how variations in a model's parameters (called input) impact its dynamics (called output), see Saltelli et al. (26). We conducted sensitivity analyses of Equations 2 and 3 to identify the parameters that most significantly influence systems dynamics. Since we focused on the parameters of the mathematical models, in that part of the paper, we did not account for the cyclic administration of the drug in our analysis. Instead, we considered the case when the initial conditions reflect a single-dose administration of CAR-T cell therapy at the onset of treatment. In addition, we treated the delay value as an additional parameter for the system described by Equation 3. For both systems, we applied the Morris method as described in Qian and Mahdi (27), a widely used approach in biomedical modeling, particularly effective for nonlinear systems with potential parameter interactions. This method evaluates both the mean absolute effect, μ_i^* ($i = 1, \dots, 11$), which indicates the average impact of the i -th parameter (either a model parameter or an initial condition) on the model outcome, and the standard deviation of the effect, σ_i , which reflects interactions or nonlinearities associated with the i -th parameter. The model outcome is defined as the average tumor cell count and CAR-T cell count over time, which serve as the basis for inferring two threshold quantities: the time at which the tumor cell population exceeds 3.5×10^{10} cells, and the time at which the CAR-T cell population drops below 1,000 cells. A high μ_i^* indicates a significant overall influence on the system, while a high σ_i highlights parameters involved in complex interactions or nonlinear behavior, contributing to variability in outcomes.

Accordingly, for both models, we plotted the rescaled values of and σ_i for each considered model output. The rescaling process involved normalizing the data by the highest value(s) across all parameters for the analyzed measure to improve data presentation. The sensitivity analysis was performed using a uniform variation range of $\pm 20\%$ around the reference values for each parameter and initial condition, see [Table 1](#).

Furthermore, in conducting the sensitivity analyses for the models, we focused on two specific (critical) thresholds: the point at which the cancer cell population grows to 3.5×10^{10} cells and the point at which the CAR-T cell population drops below 1000 cells. The justification for that choices is the following. Bogdańska et al. (28) indicated the typical astrocyte size to be approximately $10 \mu\text{m}$ in diameter, with a cell density of 10^8 cells mm^{-3} . Thus, we estimated that a tumor with a radius of about 1 cm contains approximately 3.5×10^{10} cells. This value represents one-third of the lethal tumor burden, as determined by the radius measured using magnetic resonance imaging, according to Swanson et al. (29) Woodward et al. (30). A similar critical size threshold has also been proposed in Bodnar et al. (11, 12). On the other hand, monitoring the CAR-T cell population's numbers, particularly when they fall below 1000, is crucial for predicting the patient's long-term immune response to treatment. A low CAR-T cell count suggests that the body is unable to sustain an adequate immune response, which may adversely affect survival outcomes and contribute to disease progression. For a detailed description of the algorithm used, refer to the [Supplementary Material](#).

3 Results

3.1 Numerical simulations of treatment protocols

The primary aim of developing the mathematical models was to numerically simulate the effects of glioblastoma treatment based on the therapeutic protocols outlined by Migliorini et al. (3). Considering the scope of the journal, the analytical work is provided in the [Supplementary Material](#). The following section focuses on the visualization of our key results.

For the first approach to treatment targeting the IL13R α 2 receptor (for details see Subsection 2.2.3) we see that despite the low level of drug resistance, the treatment had minimal impact, as the tumor, although growing slowly, continued to progress without showing any signs of regression, see [Figure 2](#). Notably, an immune response was observed during the initial days of treatment, evidenced by an increase in CAR-T cell levels. Interestingly, the strength of drug resistance remained consistently below 0.5 throughout treatment.

[Figure 3](#) shows the simulation results for the second approach to treatment, which targeted the HER2 receptor involving a dose of 1.89×10^6 CAR-T cells administered every six weeks. In this case, an immune system response was not observed, but the size of tumor increased steadily. [Figure 4](#) illustrates the results also for the second approach to treatment but this time with higher dose of 1.89×10^8

CAR-T cells administered less frequently – every 12 weeks. A significant tumor reduction was observed, followed by a gradual regrowth that became more pronounced after the end of treatment. Interestingly, 300 days after treatment cessation, renewed tumor regression occurred due to a second pronounced immune system response. The time to progression (TTP) was extended to 1200 days.

Simulation results for the third approach to treatment targeting EGFRvIII receptor (for details see Subsection 2.2.3) indicated that CAR-T cells exhibited peak activity between days 3 and 10 but became undetectable by day 30, [Figure 5](#), which is consistent with the behavior observed by Migliorini et al. (3). For a dose of 5×10^8 cells, the TTP was approximately 425 days.

3.2 Results on treatment protocol effectiveness

An interesting and important issue is determining how the dose size and the time interval between individual administrations affect treatment effectiveness. For this reason, we investigated how the tumor cell population response depends on the CAR-T administration schedule, specifically varying dose sizes and intervals between injections according to the description in Subsection 2.2.4.

Simulations of the first approach to treatment targeting the IL13R α 2 receptor (see Subsection 2.2.3 and Subsection 2.2.4 for details) revealed that, with a fixed total number of CAR-T cells administered – equal to 1.9×10^8 cells (note that this includes administrations in addition to the initial one of 2×10^6 cells) – increasing the number of doses while decreasing the dose size reduced the treatment's effectiveness. Shorter dosing intervals, however, resulted in a greater reduction in the tumor cell population after 540 simulation days, as shown in [Figure 6](#).

Simulation results for the second approach to treatment targeting the HER2 receptor, as described in Subsection 2.2.4, are shown in [Figure 7](#). The tumor cell population was analyzed 540 days after treatment initiation, considering varying CAR-T cell doses and dosing intervals. At the lowest dose [1.89×10^6 cells, panel (A)], tumor cell levels remained largely unchanged, even with frequent dosing (every six weeks), fluctuating around 1.25×10^{12} . The weakest effect occurred with a single dose administered 12 weeks after the initial dose. For the intermediate dose [1.89×10^7 cells, panel (B)], slight tumor reductions were observed compared to the lowest dose. Increasing dosing frequency further reduced tumor cells, with six doses every six weeks lowering the population to approximately 1.14×10^{12} . Less frequent dosing (every 12 weeks) maintained tumor levels between 1.17×10^{12} and 1.18×10^{12} . At the highest dose [1.89×10^8 cells, panel (C)], the most significant tumor reductions were seen. The best outcome, with six doses every 12 weeks, reduced tumor levels to below 1.41×10^9 . Notably, for the first two doses, higher dosing frequencies achieved better results, whereas at the highest dose, effectiveness improved with less frequent dosing.

We also analyzed TTP for the second approach to treatment as a function of the number of doses and the intervals between them,

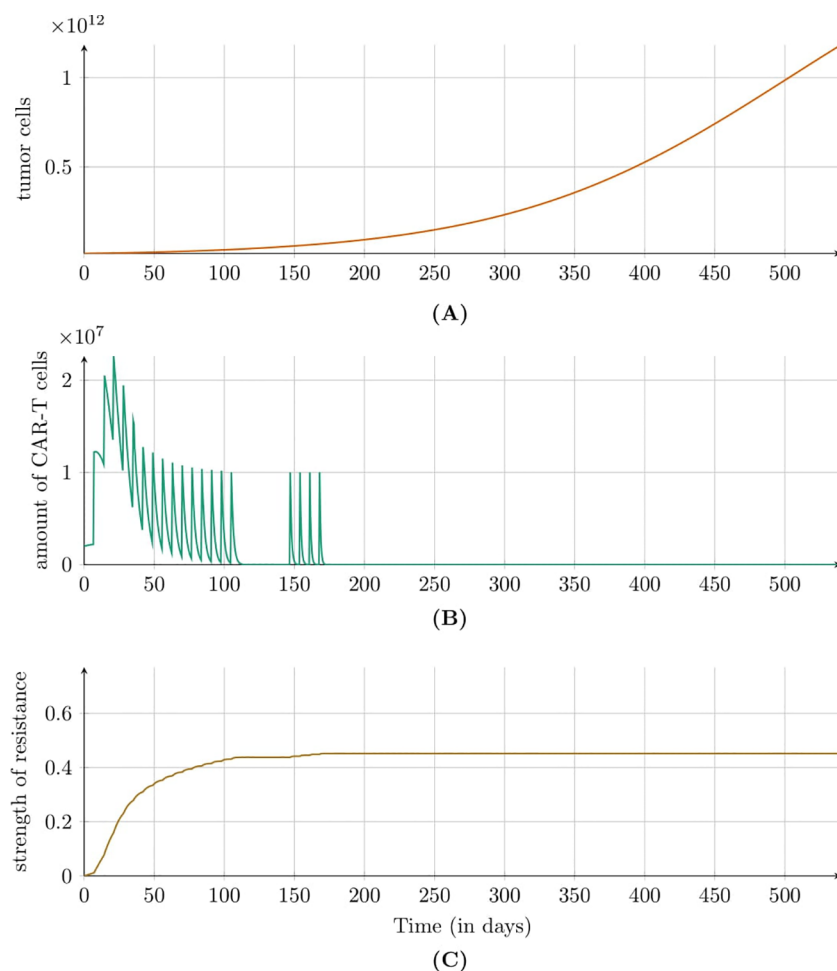


FIGURE 2

Dynamics of (A) tumor population, (B) CAR-T cell population, and (C) resistance strength modeled by Equation 2 with initial condition (5) under the first approach Migliorini et al. (3). Treatment included intracavitary CAR-T cell infusions via a Rickham catheter. Parameters and initial conditions are in Table 1, except $C_0 = 2 \times 10^6$ CAR-T cells and the treatment schedule detailed in Subsection 2.2.3.

as outlined in Subsection 2.2.4. Our analysis focuses on a dose of 1.89×10^8 , identified in previous simulations as the most effective. Notably, the longest TTP was observed with six doses administered every 12 weeks, while a slightly shorter TTP was achieved with five doses at the same interval, as shown in Figure 8. Interestingly, the addition of the fifth and sixth doses in the 12-week schedule significantly extended TTP by over 500 days. This improvement correlates with renewed tumor regression, driven by a second pronounced immune system response, which is shown in Figure 4.

We evaluated the effectiveness of CAR-T cell treatment protocols involving seven equal doses – 7.23×10^7 , 1×10^8 , and 1.89×10^8 cells – administered at intervals ranging from 1 to 15 weeks, as shown in Figure 9. The best outcome was achieved with the lowest dose (7.23×10^7 cells) administered every 15 weeks, resulting in a TTP of 2140 days. For intervals of 1 to 6 weeks, the highest dose (1.89×10^8 cells) was most effective, followed by the medium dose (1×10^8 cells) and the lowest dose. However, with a 7-week interval, the ranking shifted, and the lowest dose provided the longest TTP of 994 days. At an 8-week interval, the medium dose (1×10^8 cells) slightly outperformed the lowest dose, with TTPs of 992

and 942 days, respectively. For intervals of 9 to 15 weeks, the lowest dose consistently yielded the best outcomes, while the highest dose resulted in the shortest TTP.

To understand the seemingly counterintuitive simulation result – where lower doses outperform higher doses at longer intervals – we performed additional time-solution simulations for the specified treatment protocols with intervals of 5, 10, and 15 weeks. Results for the 15-week intervals are provided in the *Supplementary Material*, see *Supplementary Figure S5*. In Figure 10, we examined the administration of seven doses of CAR-T cells with sizes 7.23×10^7 , 1×10^8 , and 1.89×10^8 at 5-week intervals. The simulations revealed that each dose rapidly reduces the tumor cell population, followed by regrowth once CAR-T cells were no longer detectable in the body. The CAR-T cell population dynamics were similar across all dose sizes, likely due to the immunological response occurring at similar times. Notably, the highest dose (1.89×10^8) most effectively delayed the tumor's return to its original size.

A different behavior is observed in Figure 11, where seven doses of CAR-T cells were administered every 10 weeks. As before, each dose of CAR-T cells reduced the tumor cell population; however,

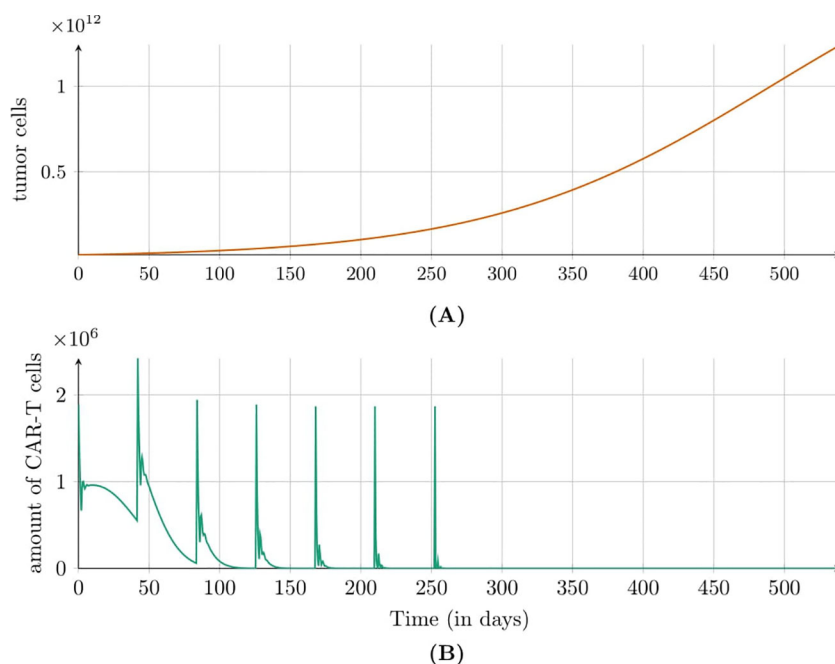


FIGURE 3
 Dynamics of (A) tumor and (B) CAR-T cell populations modeled by Equation 3 with initial conditions (6) and (7) under the second approach Migliorini et al. (3). Treatment involved cyclic injections of 1.89×10^6 HER2/CMV CAR-T cells every six weeks. Simulations assume a 70kg, 180cm patient. Parameters and initial conditions are in Table 1, except $C_0 = 1.89 \times 10^6$ and the treatment schedule detailed in Subsection 2.2.3.

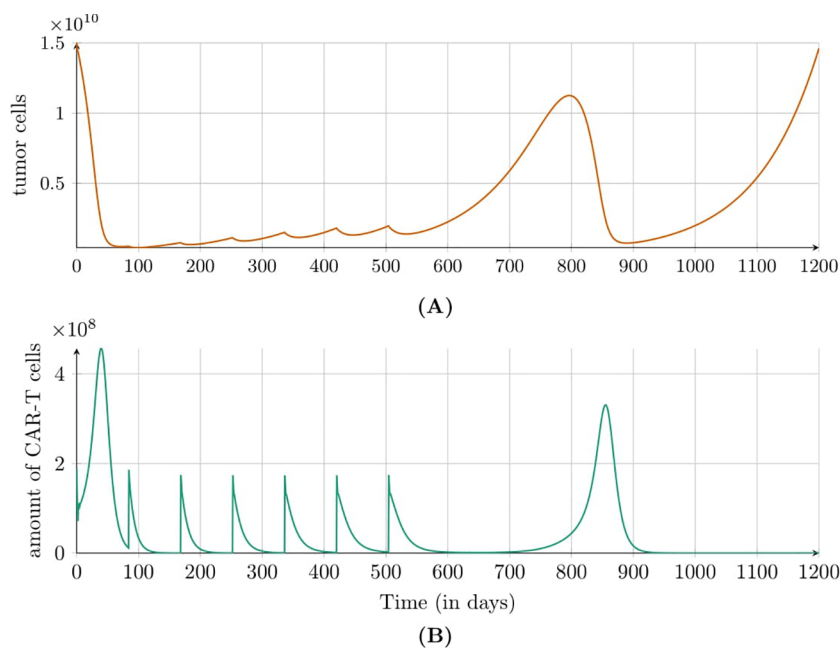


FIGURE 4
 Dynamics of (A) tumor and (B) CAR-T cell populations modeled by Equation 3 with initial conditions (6) and (7) under the second approach Migliorini et al. (3). Treatment included cyclic injections of 1.89×10^8 HER2/CMV CAR-T cells every 12 weeks. Simulations assume a patient weight of 70kg and height of 180cm. Parameters and initial conditions are listed in Table 1, except C_0 set to 1.89×10^8 , and the treatment schedule detailed in Subsection 2.2.3.

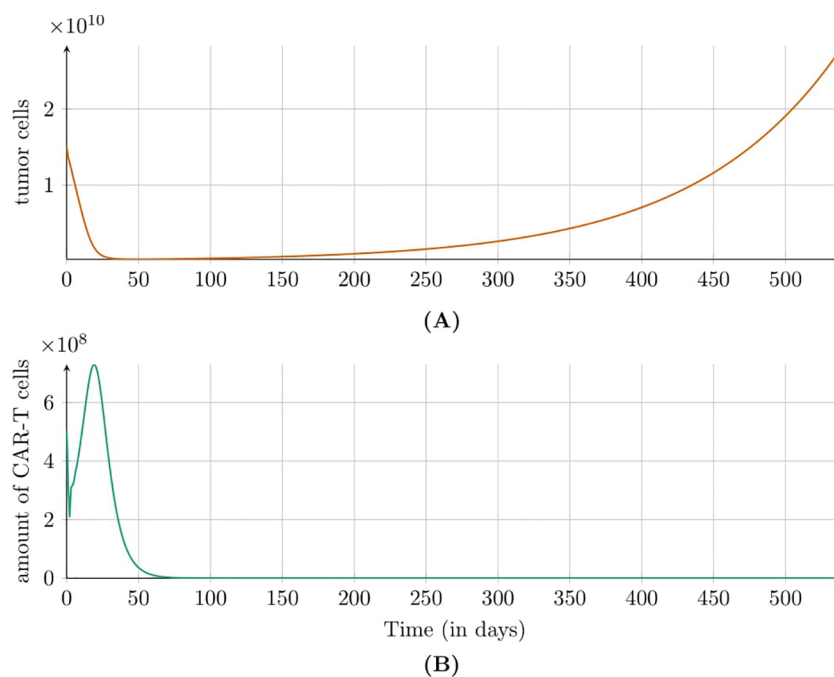


FIGURE 5
Dynamics of (A) tumor and (B) CAR-T cell populations modeled by Equations 3 with initial conditions (6) and (7) under the third approach Migliorini et al. (3). Treatment involved a single injection of 5×10^8 EGFRvIII CAR-T cells. Parameters and initial conditions are listed in Table 1, with C_0 marked by (☆☆) and the schedule detailed in Subsection 2.2.3.

the subsequent dynamics varied significantly. For the highest dose of 1.89×10^8 , we observed the fastest tumor recurrence. In contrast, the two lower doses resulted in oscillatory behaviors that ultimately lead to exponential tumor growth. Tumor regrowth to its original size occurred latest with the lowest dose of 7.23×10^7 . The CAR-T cell population also exhibited interesting dynamics. For the highest dose, the CAR-T cell population rapidly declined to zero. However, the two lower doses induced oscillatory dynamics, similar to the tumor population, resulting in consecutive immune responses to

treatment. Notably, for the lowest dose, we observed the longest cumulative treatment effect, with the CAR-T cell population disappearing only after 1200 days.

3.3 Sensitivity analysis results

The sensitivity analysis for the tumor cell population T was conducted using the Morris method for two models: Equation 2

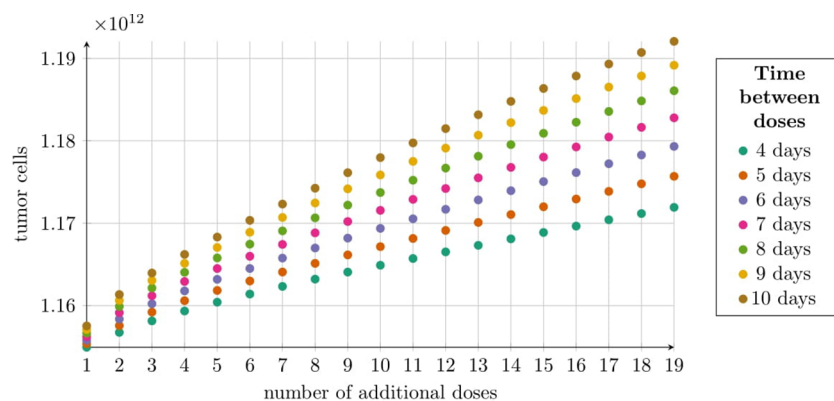


FIGURE 6
Tumor size at 540 days post-treatment under the first approach Migliorini et al. (3), modeled by Equation 2 with initial condition (5). Treatment began with 2×10^6 CAR-T cells followed by 19 variable doses, totaling 1.9×10^8 additional CAR-T cells (Subsection 2.2.4). The horizontal axis shows the number of CAR-T cell doses, with dosing intervals (4–10 days) indicated by colors in the legend. The vertical axis represents average tumor cell count at 540 days. Simulation parameters are in Table 1, except $C_0 = 2 \times 10^6$ CAR-T cells. Cyclic doses were calculated using Equation 8.

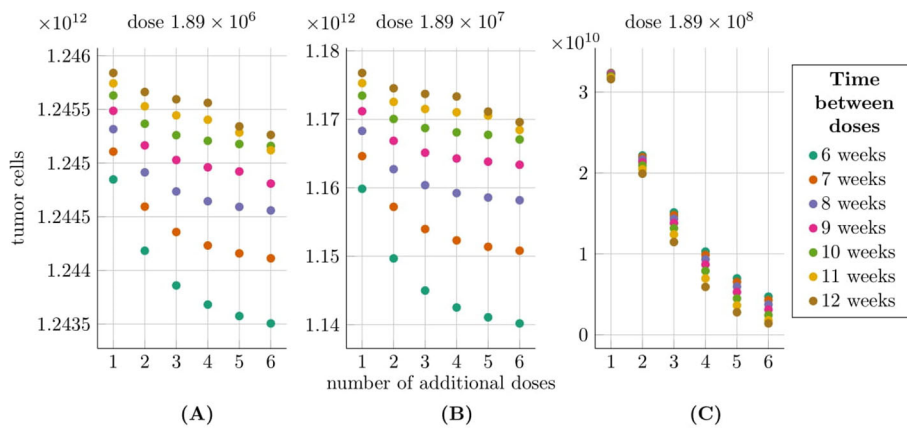


FIGURE 7

Tumor size at 540 days post-treatment under the second approach Migliorini et al. (3), modeled by Equation 3 with initial conditions (6) and (7), accounting for varying dose sizes and dosing intervals. The horizontal axis shows the number of additional CAR-T doses (excluding the initial dose), with colors indicating dosing intervals (6–12 weeks). The vertical axis represents the average tumor size 540 days after treatment initiation. Plots correspond to dose sizes: (A) 1.89×10^6 , (B) 1.89×10^7 , and (C) 1.89×10^8 cells. Treatment was administered to a patient weighing 70 kg and measuring 180 cm, as described in Migliorini et al. (3). The simulation parameters are provided in Table 1, except for C_0 , which is the same as the considered dose size in each of the three scenarios.

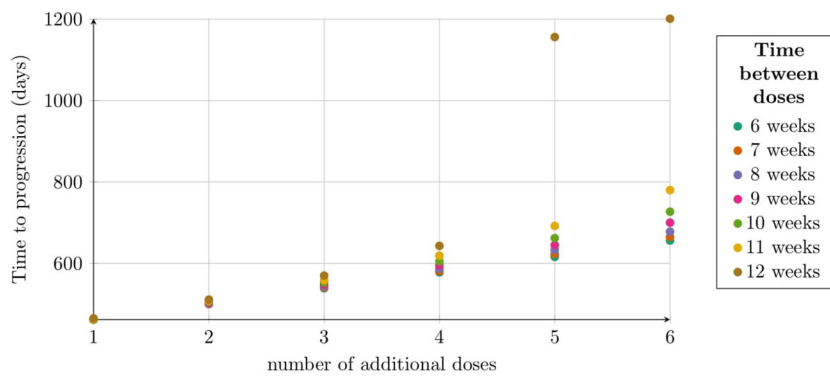


FIGURE 8

TTP distribution under the second approach, illustrating the impact of dose number and interval size. Each dose contained 1.89×10^8 CAR-T cells. The horizontal axis shows the number of doses, with colors indicating dosing intervals (6–12 weeks). The vertical axis represents TTP (days). Simulation parameters are in Table 1, except $C_0 = 1.89 \times 10^8$.

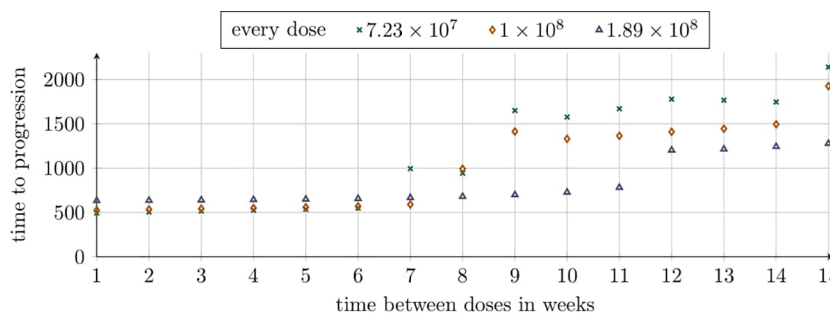


FIGURE 9

TTP distribution under the second approach, reflecting varying dosing intervals across simulations with constant intervals per simulation. Each simulation evaluates six additional doses of sizes 7.23×10^7 , 1×10^8 , and 1.89×10^8 . The horizontal axis represents dosing intervals (1–15 weeks), with markers indicating dose sizes as shown in the legend. The vertical axis represents TTP (days). Simulation parameters are detailed in Table 1, except C_0 which matches the dose size for each scenario.

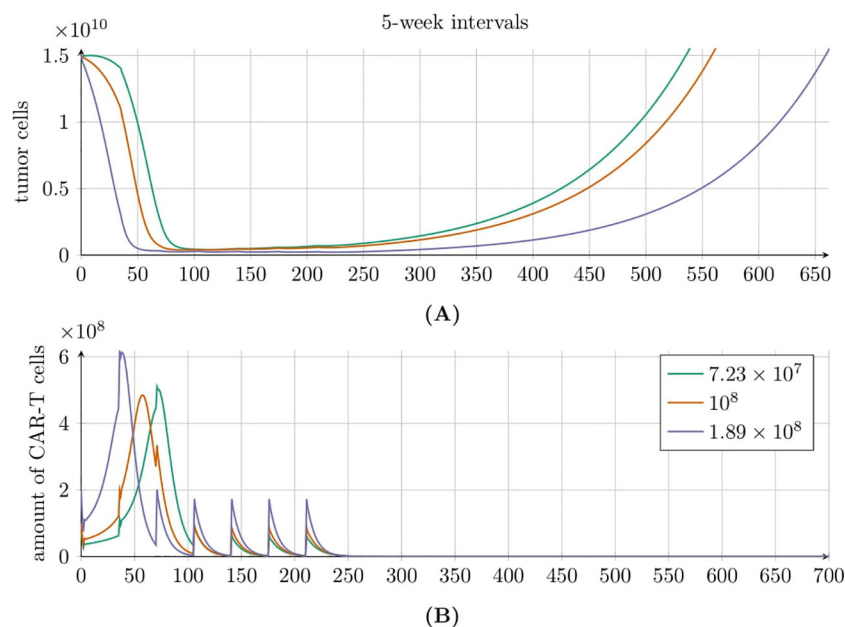


FIGURE 10
Tumor (A) and CAR-T cell (B) population dynamics modeled by Equation 3 with initial conditions (6) and (7), under the second approach Migliorini et al. (3). Seven equal doses of HER2/CMV CAR-T cells were administered at 5-week intervals, with individual dose sizes of 7.23×10^7 (green line), 1×10^8 (red line), and 1.89×10^8 (purple line) cells. Parameters and initial conditions are provided in Table 1, except for C_0 which matches the dose size for each of the three scenarios.

with initial conditions described by Equations 3 and Equation 5 with initial conditions described by Equations 6 and 7. Details of the methodology are provided in Subsection 2.2.6 and the Supplementary Material. Comprehensive results for the CAR-T

cell population C are also available in the Supplementary Material. Sensitivity analysis was performed over the entire time course (for details, see the Supplementary Material). However, in the main text, we present results only for three representative times

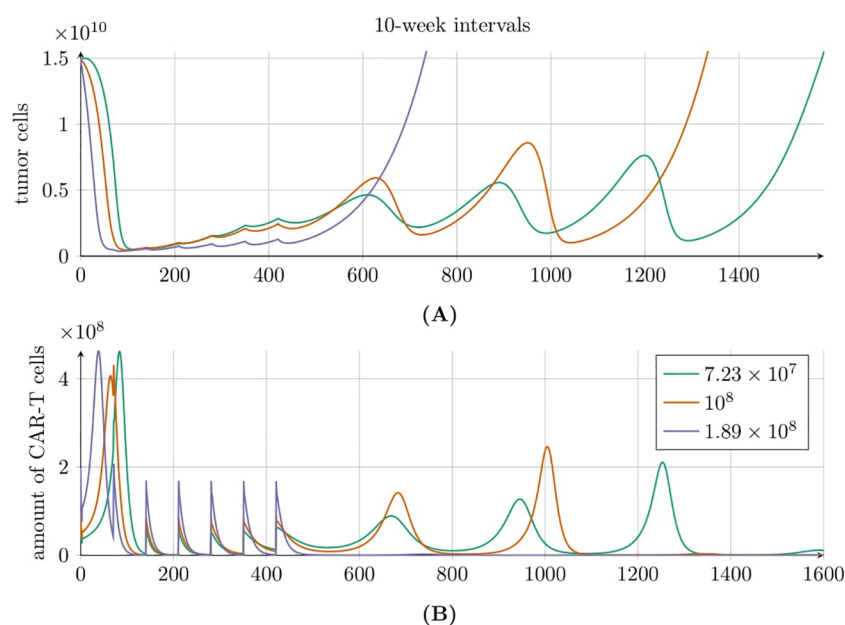


FIGURE 11
Tumor (A) and CAR-T cell (B) population dynamics modeled by Equation 3 with initial conditions (6) and (7), under the second approach Migliorini et al. (3). Seven equal doses of HER2/CMV CAR-T cells were administered at 10-week intervals, with individual dose sizes of 7.23×10^7 (green line), 1×10^8 (red line), and 1.89×10^8 (purple line) cells. Simulations assume a 70kg, 180cm patient. Parameters and initial conditions are provided in Table 1, except for C_0 which matches the dose size for each of the three scenarios.

– 180, 360, and 540 days post-administration – and for two thresholds: the time for the tumor to reach 3.5×10^{10} cells, and the time until the CAR-T cell population drops below 1,000 cells.

3.3.1 Sensitivity analysis results for the model with drug resistance

We analyzed the impact of individual parameters and initial conditions on the tumor cell population over time, based on Equation 2 with initial condition (5) (see Supplementary Figure S6 in Supplementary Material). In Figure 12 we presented results for three time points corresponding to 180, 360, and 540 days. Across all observed time points, the parameter ρ_T had the greatest influence on the tumor cell population size. At 180 and 360 days, the second and third most influential factors were the initial tumor cell count T_0 and the maximum tumor size K , respectively. However, after 540 days, the rankings of these two parameters had swapped. Other parameters had a significantly smaller impact on the tumor cell population size. Among these, the initial number of CAR-T cells C_0 and the parameter α_T describing the effective inactivation of CAR-T cells by the tumor had the smallest impact. In the Supplementary Material a comprehensive sensitivity analysis of both variables is presented, covering the period from day 0 (treatment initiation) to 540 days (1.5 years), see Supplementary Figures S6 and S7.

Figure 13 illustrates the impact of parameter variations and initial conditions on two critical thresholds. Panel (A) depicts the effect of these variations on the time required for the tumor to reach the critical threshold of 3.5×10^{10} tumor cells, while panel (B) shows their effect on the time until the CAR-T cell population declined below the critical threshold of 1000 cells. Among the analyzed factors, the initial tumor size T_0 was identified as the most influential determinant of the time to exceed the critical threshold for the tumor variable T . The tumor growth rate ρ_T exhibited a nearly equal impact. In contrast, other parameters had considerably smaller effects, with ρ_C , governing the proliferation rate of CAR-T

cells, showing the least influence on the time required for the tumor to reach its critical threshold. Regarding the variable C and the time at which the CAR-T cell population falls below the critical threshold of 1000 cells, the most influential parameter was α_C , representing the inactivation rate of CAR-T cells. Notably, the tumor growth rate ρ_T and the initial tumor size T_0 , both critical for determining the time required for the tumor to reach its strategic threshold, also had significant effects in this context. This finding highlights the interconnected dynamics between the tumor and CAR-T cells. Another key parameter was α_R , which represents the strength of drug resistance and underscores its crucial role in shaping treatment outcomes as modeled by Equation 2. In contrast, the CAR-T half-saturation level g_C had the least influence.

3.3.2 Sensitivity analysis results for the model with time delay

Following the methodology presented in Subsection 2, we performed a series of simulations to study how changes in parameter values and initial conditions influence the tumor cell population. These simulations were based on Equation 3 with initial conditions specified in Equations 6 and 7, evaluated at three time points: 180, 360, and 540 days, see Figure 14. After 180 days, α_C , representing the inactivation rate of CAR-T cells, exhibited the greatest influence on tumor population size. The next most influential parameters were the tumor half-saturation level g_T and the mean lifetime of active CAR-T cells at the tumor site, τ_C . The remaining parameters had a comparable impact on the dynamics of the tumor population, except for α_T , which describes the effective inactivation of CAR-T cells by the tumor. This parameter had the least effect at this time point. Similar trends were observed after one year, with the tumor growth rate ρ_T and τ_C gaining importance. By 540 days, however, ρ_T and g_T emerged as the most critical determinants of tumor population dynamics. Notably, the parameters α_C and τ_C continued to play a significant role. An

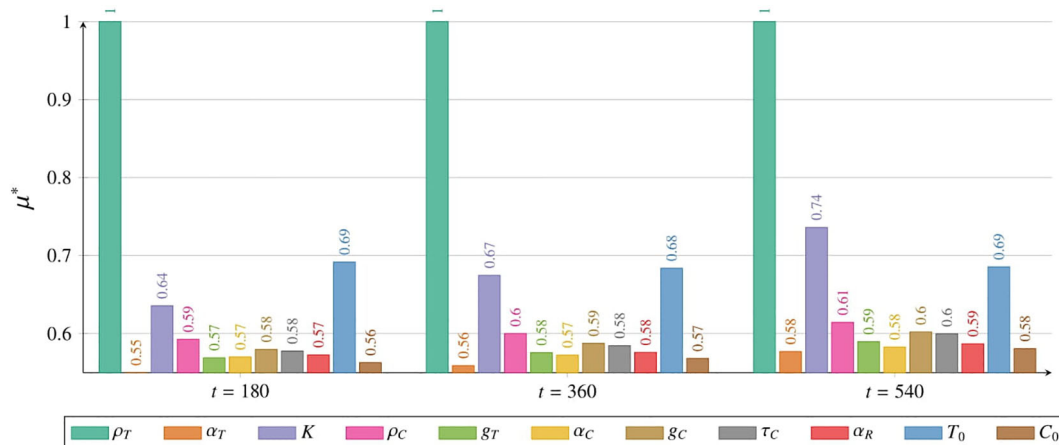


FIGURE 12 Impact of individual parameters and initial conditions on the tumor cell population, measured by μ^* (details in Subsection 2.2.6), as described by Equations 2 with initial condition (5), with a single CAR-T cell dose administered at $t = 0$. Results are shown for 180 days (left), 360 days (middle), and 540 days (right). Colors represent parameters or initial conditions as indicated in the legend. Simulation parameters are listed in Table 1, with C_0 marked as (\star).

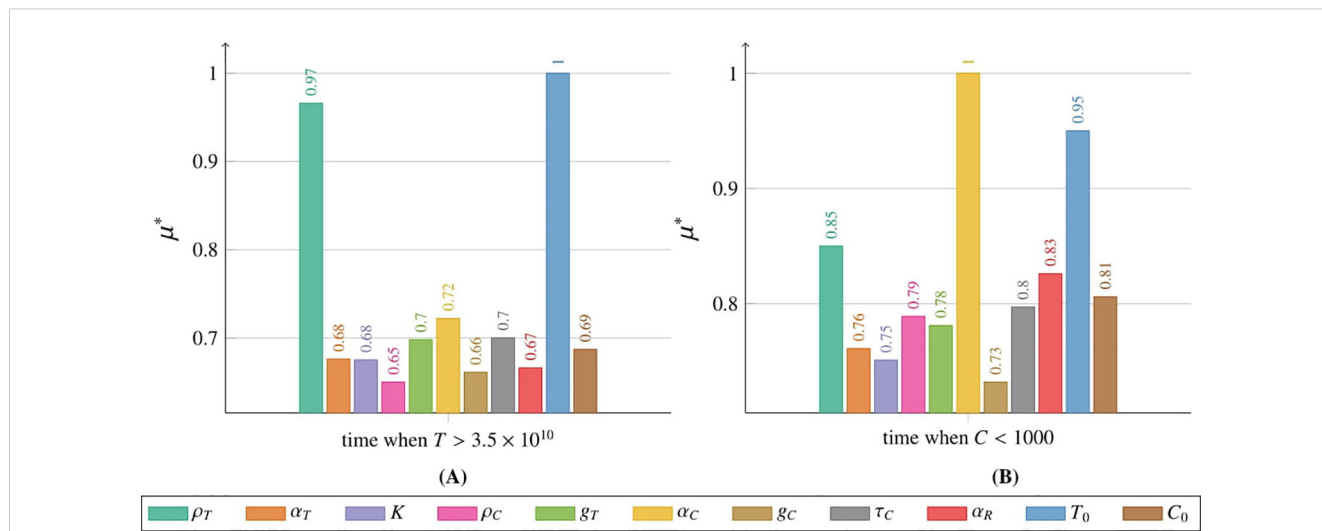


FIGURE 13 Impact of individual parameters and initial conditions on the tumor cell population, measured by μ^* (details in Subsection 2.2.6), as described by Equation 2 with initial condition (5), with a single CAR-T cell dose administered at $t = 0$. (A) Effect on T when the tumor population reaches 3.5×10^{10} cells, (B) effect on C when the CAR-T population drops below 1000 cells. Colors represent parameters and initial conditions, as per the legend. Simulation parameters are in Table 1, with C_0 marked as (\star).

interesting observation at the last time point was the increased importance of the initial CAR-T cell value, C_0 , and the α_T parameter. Additionally, ρ_C , which governs the CAR-T cells proliferation, had the least impact on tumor population dynamics at this stage. The Supplementary Material include a detailed sensitivity analysis conducted from day 0 (the start of treatment) to day 540 (corresponding to 1.5 years) for both variables, see Supplementary Figures S9 and S10. In addition to comprehensive plots for the measure, the materials also provide detailed plots for the σ_T measure. For further details, see Subsection 2.2.6.

We also investigated how variations in parameter values and initial conditions influence the time required for the tumor

population to reach the critical threshold of 3.5×10^{10} cells (Figure 15A) and the time at which the CAR-T cell population falls below 1000 cells (Figure 15B). The parameter with the greatest influence on the time for variable T to reach the critical threshold of 3.5×10^{10} tumor cells was τ_C , which represents the mean lifetime of active CAR-T cells at the tumor site. This was followed by ρ_T and g_T , which correspond to the tumor growth rate and the tumor half-saturation level, respectively. Interestingly, τ , representing the average time required to initiate CAR-T cell production in the body, and K , denoting the maximum tumor size, had the least impact on the tumor population threshold. Conversely, g_T exerted the most significant influence on the time at which the CAR-T cell

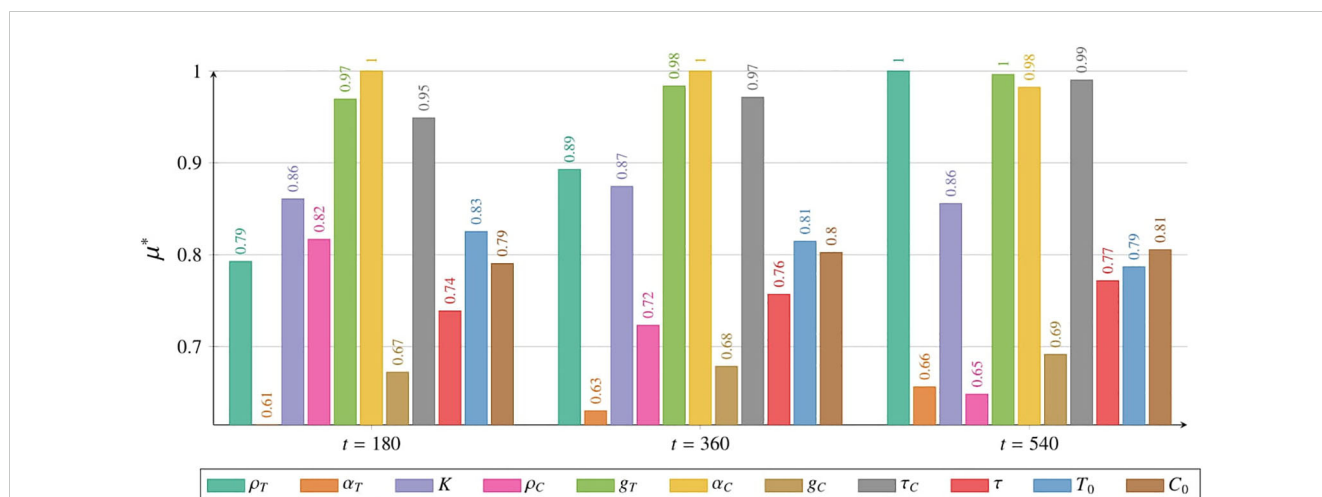
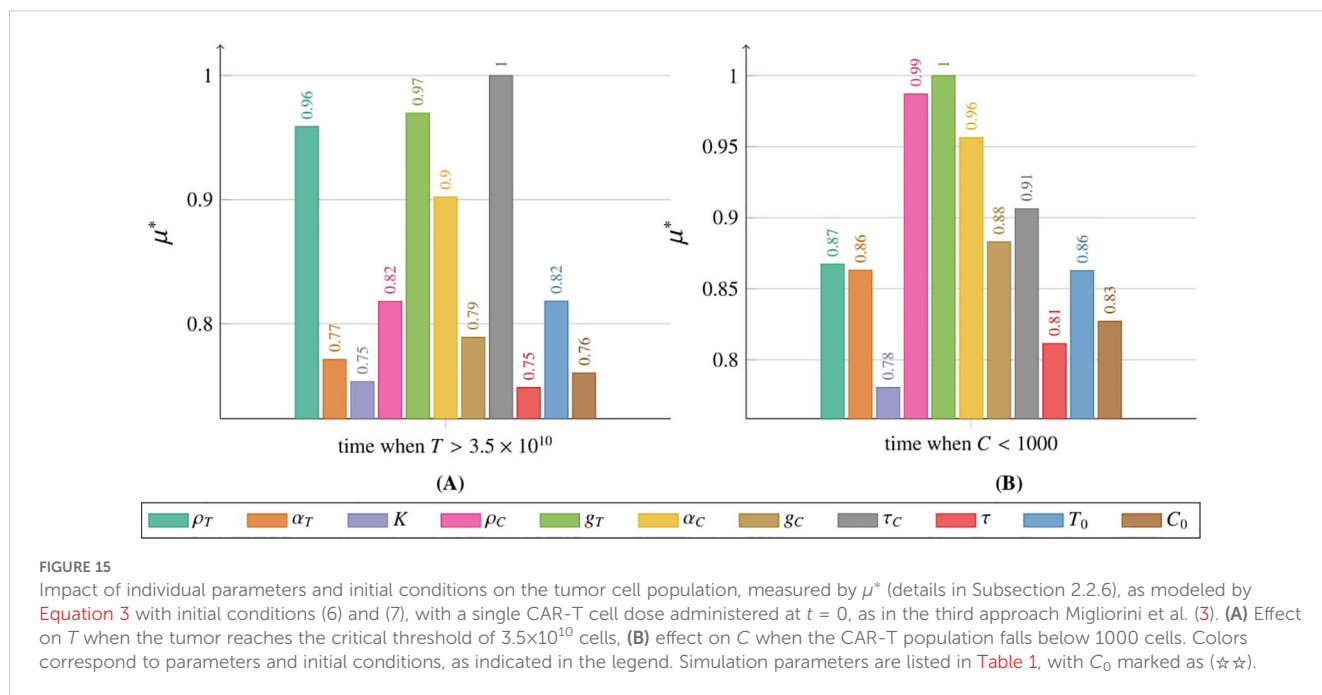


FIGURE 14 Impact of individual parameters and initial conditions on the tumor cell population, measured by μ^* (details in Subsection 2.2.6), as described by Equation 3 with initial conditions (6) and (7), with a single CAR-T cell dose administered at $t = 0$, as in the third approach Migliorini et al. (3). Results are shown for 180 days (left), 360 days (middle), and 540 days (right). Colors represent parameters or initial conditions, as indicated in the legend. Simulation parameters are listed in Table 1, with C_0 marked as (\star).



population fell below the critical threshold of 1000 cells. Notably, ρ_C , which defines the CAR-T cell proliferation rate, exhibited a nearly comparable impact. In contrast, K was the least influential parameter in this context.

3.4 Supporting results

In the **Supplementary Material**, we provide additional analytical results related to models (2) and (3) under cyclic administration of CAR-T cells. These results are not included in the main text as they are not central to the primary focus of the study. We also present numerical illustrations demonstrating the impact of resistance (**Supplementary Figures S1, S2**) and time delay (**Supplementary Figures S3, S4**) on the model dynamics.

4 Discussion

Analyzing the simulation results for Equation 2 with initial condition (5), modeling the first approach to glioblastoma treatment (see Subsection 1.1), revealed a critical insight: the emergence of drug resistance effectively nullified the therapeutic effect. All tested dosing regimens produced similar outcomes within the assumed parameters range, as the rapid emergence of resistance rendered the therapy ineffective, see Figure 2. This finding aligns with clinical observations, where patients initially responded favorably to treatment but soon experienced diminishing therapeutic benefits. Therefore a deeper understanding of the resistance phenomenon is essential for accurately modeling disease dynamics and assessing treatment effectiveness. As an initial step, incorporating a delayed onset of drug resistance into the model could offer valuable insights. However, due to the lack of

precise data on the timing of this delay, we opted to proceed with a simplified model that omits this feature. Exploring the delay duration and other characteristics of the resistance phenomenon is deferred to future research.

Regarding intravenous administration, as employed in the second and third approaches to treatment, clinical studies indicated that while the initial effects may be less pronounced, this method demonstrated greater long-term efficacy, particularly at higher and multiple doses. Figures 3, 4 illustrate simulations of treatment following the second approach, enabling an *in silico* comparison of therapeutic efficacy at low and high doses, respectively. Administering a single dose at the start of treatment, as in the third approach (see Figure 5), or insufficient dosing in the second approach failed to achieve significant tumor reduction. However, higher doses in the second approach yielded improved outcomes, especially when delivered through multiple administrations. This strategy resulted in a longer TTP compared to single-dose regimens, emphasizing the importance of optimizing dosing strategies, which can be effectively explored *in silico*.

4.1 Discussion on the effectiveness of treatment protocols

Treatment approaches based on the cyclic administration of CAR-T cells showed significant promise for improving therapeutic effectiveness. This was particularly true for the second approach, where the impact of resistance was less pronounced, although some conclusions can also be drawn for the first approach. Simulations highlighted the advantages of administering higher doses at shorter intervals, as illustrated in Figure 6. This effect was likely associated with the induction of resistance to treatment. For IL13R α 2 receptor-targeted therapy, the optimal strategy may be to

maximize tumor reduction with high doses of CAR-T cells while they remain effective, that is, before resistance develops.

In pursuit of guidelines for more effective therapeutic procedures, we focused particularly on the second approach to treatment. The analysis of simulations with varying dosages, as shown in [Figure 7](#), yielded several notable conclusions. For the lowest dosage considered (1.89×10^6 cells) and the moderate dosage (1.89×10^7 cells), the optimal strategy was to administer CAR-T cells as frequently as possible. In contrast, the highest dosage (1.89×10^8 cells) achieved the best results when administered less frequently, approximately every 12 weeks. This discrepancy likely arose because smaller doses may be insufficient to significantly inhibit tumor growth or effectively stimulate CAR-T cell proliferation. In such cases, frequent administration helped maintain a minimum therapeutic concentration, preventing excessive tumor regrowth between doses and gradually weakening the tumor cell population. Consequently, frequent administration of smaller doses became crucial for achieving any therapeutic effect. Conversely, higher doses allowed entry into the optimal therapeutic window, where a balance was achieved between tumor cell destruction and CAR-T cell proliferation. This ensured maximum effectiveness, eliminating a substantial portion of the tumor while minimizing strain on the body and avoiding premature tumor saturation. Thus, higher doses administered at appropriately longer intervals yielded superior outcomes compared to frequent administration of high concentrations, which can reduce overall treatment efficacy.

While investigating the optimal therapeutic outcome for the highest dose considered, 1.89×10^8 CAR-T cells, we identified several noteworthy conclusions regarding TTP. The most promising results were observed with five and six doses administered at 12-week intervals, yielding TTP values of 1156 and 1201 days, respectively. These values were significantly higher than those achieved with other administration schedules (see [Figure 8](#)). Such elevated TTP values were likely attributable to the secondary induction of an immune response – CAR-T cell activation triggered by the moderate regrowth of the tumor while sufficient CAR-T cells remained present to initiate the response. Regular administration of CAR-T cells at 12-week intervals appeared to optimize their therapeutic potential by balancing tumor cell elimination with CAR-T cell activation, effectively maintaining CAR-T cells at a therapeutic level. An intriguing observation was that with a small number of additional doses – particularly a single additional dose – the TTP remained relatively consistent regardless of the dosing interval. These findings underscored the importance of both the number of doses and the dosing interval as critical parameters influencing the efficacy of CAR-T therapy. Repeated, regular administration of CAR-T cells at carefully selected intervals yielded the most favorable therapeutic outcomes.

Exploring the role of intervals between CAR-T cell administrations within the framework of the second approach to treatment revealed valuable insights. With fixed dose sizes (7.23×10^7 , 1×10^8 , and 1.89×10^8 cells) administered over seven cycles, therapeutic efficacy highly depended on the time between

administrations, see [Figure 9](#). The most significant finding was that increasing the intervals between administrations and using a smaller dose led to better therapeutic outcomes. Specifically, the best result was achieved with the dose of 7.23×10^7 cells (the smallest of the three doses considered) when administered every 15 weeks (the longest interval examined), resulting in a TTP of 2140 days.

To shed more light on the dynamics of tumor and CAR-T cell populations under the second approach to treatment and to better understand this counterintuitive result, we conducted additional numerical simulations of model [Equation 3](#) with initial conditions specified in [Equations 6](#) and [7](#), exploring varying dose sizes and administration intervals. [Figure 10](#) presents results for CAR-T cell administrations at 5-week intervals. In this scenario, lower CAR-T cell doses failed to reduce tumor cell levels sufficiently, resulting in suboptimal treatment outcomes, whereas higher doses yielded better results. In contrast, [Figure 11](#) shows results for 10-week intervals. Here, larger CAR-T doses caused a faster and deeper reduction in the tumor population and maintained it at low levels for longer. However, because CAR-T cell proliferation depended on the presence of tumor cells, excessive tumor suppression led to insufficient proliferation of new CAR-T cells and a rapid decline in their levels. Paradoxically, therefore, higher doses overly suppressed tumor cells, weakening the immune response and eventually depleting CAR-T cells. This loss of immune control allowed tumor cells to proliferate unchecked. Conversely, smaller doses maintained tumor cells at levels that are low enough to slow disease progression but high enough to sustain immune system activity, resulting in a longer TTP.

The results resemble those observed in the metronomic approach to chemotherapy, which suggests that for malignant cancers, smaller, sub-maximal drug doses may outperform maximum tolerated doses in extending survival [Scharovsky et al. \(14\)](#); [Kareva et al. \(31\)](#); [Ledzewicz and Schättler \(32\)](#); [Bajger et al. \(33, 34\)](#); [Bodzioch et al. \(35\)](#). Modeling CAR-T therapy reveals similar dynamics, emphasizing the potential to optimize dosing intervals and quantities to maximize TTP. Future clinical research should focus on capturing the cumulative immune response to validate these predictions.

4.2 Discussion on the sensitivity analysis

Sensitivity analysis underscores the importance of patient-specific parameters in therapy efficacy. Accurate estimation of these parameters before treatment is crucial for personalizing dosing strategies. This aligns with previous immunotherapy studies [Kronik et al. \(36\)](#); [Kogan et al. \(37\)](#). Precise parameter assessment can help determine the optimal dose and interval to maximize therapeutic outcomes. [Figure 12](#) shows that the tumor growth rate parameter ρ_T significantly impacted the tumor cell population in [Equation 2](#) with initial condition (5), underscoring the role of tumor aggressiveness in disease progression. A high ρ_T indicates rapid tumor growth, making early treatment control more challenging. In later therapy stages, the maximum tumor size

parameter K became more influential. However, this parameter remains beyond direct therapeutic control.

The dominant factors influencing the CAR-T cell population shifted over time. Initially, the starting CAR-T cell count C_0 was most critical, highlighting the importance of dose selection for effective treatment. As therapy progressed, other parameters became more influential (see [Supplementary Figure S7](#) in the [Supplementary Material](#)). After one year, the maximum tumor size K had the greatest impact, affecting both CAR-T cell proliferation ρ_C and drug resistance α_R . By day 540, α_T , which controls tumor cell elimination by CAR-T cells, became the key factor. At this stage, the minimal influence of τ_C (CAR-T cell decay rate) reflected the low CAR-T cell count, reducing therapeutic effectiveness. The rising impact of α_R in later stages highlights the need for strategies to overcome drug resistance. Enhancing CAR-T cell survival and expansion in the tumor microenvironment could significantly improve treatment outcomes and support long-term remission. However, it should be marked that this result is not so strong as for the variable T because of the dynamic changes in the order of most influential parameters in time; cf. [Supplementary Figure S8](#) in the [Supplementary Material](#).

Sensitivity analysis of [Equation 3](#) with initial conditions (6) and (7) revealed differences in parameter influence on tumor and CAR-T cell dynamics compared to [Equation 2](#) (see [Figure 14](#)). Both models simulated a single CAR-T cell dose administered at $t = 0$, but in [Equation 3](#), the tumor cell population after 180 and 360 days was most influenced by the CAR-T cell inactivation rate α_C , highlighting the importance of preserving the CAR-T cell population early in therapy to control tumor size. After 540 days, as the CAR-T cell population greatly diminished, [Figure 5](#), the tumor growth rate ρ_T became the primary driver of tumor expansion. Since ρ_T reflects patient-specific tumor aggressiveness, targeting it during therapy could be vital for improving outcomes. Over time, the average CART cell production time τ_C became more important, suggesting that prolonging CAR-T cell persistence may enhance tumor control. In contrast, the tumor elimination rate by CAR-T cells α_T was least influential during the first year, highlighting that early therapy challenges are more about maintaining CAR-T cell activation and survival than immediate tumor-killing efficiency. Although initially very important, after 1.5 years, the CAR-T cell proliferation rate ρ_C became the least significant factor, likely due to the decline in the CAR-T cell population and its resulting minimal impact on tumor control.

The CAR-T cell population after 180 days was most influenced by g_T , the tumor half-saturation parameter, which correlates with tumor immunogenicity (higher values indicate a more effective immune response across tumor sizes, see [Supplementary Figure S11](#) in [Supplementary Material](#)). After 360 days, τ_C became the key parameter, reflecting the importance of CART cell viability. After 540 days, ρ_C emerged as the most influential factor, underscoring the role of CAR-T cell regeneration for sustained therapeutic efficacy. The least significant parameter after 540 days was α_T , as in the first approach, indicating that tumor elimination remained essential regardless of the treatment strategy. These scenarios require further *in silico* and *in vivo* investigation to explore how less aggressive tumors

may impact CAR-T therapy dynamics. Future studies could also test model-predicted dosing regimens, which may enhance outcomes, as suggested by previous research [Kronik et al. \(36\)](#); [Kogan et al. \(37\)](#).

4.3 Conclusions

In conclusion, we emphasize that the proposed mathematical models successfully reproduce the clinical trial results described by [Migliorini et al. \(3\)](#). Additionally, these models enable the exploration of various treatment protocols prior to initiating clinical trials. However, we acknowledge the limitations of our models, primarily stemming from simplifying assumptions. First, our models account for only two components of the immune response – tumor cells and CAR-T cells – whereas real immune reactions involve numerous, more complex interactions. Second, the tumor growth function is assumed to be logistic, but with appropriate clinical data for glioblastoma, the growth function should be fitted to those data, possibly leading to a different type of growth model. Third, the models do not incorporate spatial considerations, which could capture exogenous tumor heterogeneity influenced by factors such as oxygen and glucose supply.

Endogenous factors, such as epigenetics and therapy sensitivity (e.g., related to antigen exposure), further contribute to tumor heterogeneity, which is not addressed in our current approach. In the context of heterogeneity, tumor resistance can be described in greater detail by incorporating tumor cells with varying resistance properties.

Moreover, the models require improved calibration, as the results presented here are qualitative. Incorporating patient-specific data could enhance the models' accuracy, enabling quantitative predictions and broader clinical applicability.

In the context of personalized medicine, greater efforts should be made to better specify patient-specific model parameters. Thus far, we have conducted sensitivity analysis only for a single-dose regimen, while our results underscore the effectiveness of multiple-dose protocols. Therefore, future work should include sensitivity analysis tailored to multiple dose regimens. Additionally, the modeling of resistance to therapy could be enhanced. For instance, including the delayed triggering of the resistance or incorporate a division of the tumor population into subpopulations of sensitive and resistant cells, allowing for a more accurate representation of tumor heterogeneity and treatment response.

Despite the limitations discussed, we hope that our findings will contribute to the improved application of CAR-T therapy in treating gliomas and other solid tumors. The proposed models are highly versatile and can be adapted to suit specific cases, offering a valuable framework for exploring and optimizing treatment strategies.

Data availability statement

The original contributions presented in the study are included in the article/[Supplementary Material](#). Further inquiries can be directed to the corresponding author.

Ethics statement

Ethical approval was not required for the study involving humans in accordance with the local legislation and institutional requirements. Written informed consent to participate in this study was not required from the participants or the participants' legal guardians/next of kin in accordance with the national legislation and the institutional requirements.

Author contributions

MS-L: Formal Analysis, Visualization, Writing – original draft, Writing – review & editing, Investigation, Software. ZS: Conceptualization, Methodology, Writing – original draft, Writing – review & editing. MP: Formal Analysis, Investigation, Methodology, Writing – review & editing. MB: Methodology, Software, Visualization, Writing – review & editing. UF: Supervision, Writing – review & editing, Conceptualization, Methodology.

Funding

The author(s) declare that financial support was received for the research and/or publication of this article. This work was supported by the Excellence Initiative – Research University program (2020–2026) at the University of Warsaw, Poland. ZS was partially supported by the National Science Centre, Poland, grant UMO-2024/54/A/ST1/00159.

Acknowledgments

Z.S. was partially supported by the National Science Centre, Poland, grant UMO-2024/54/A/ST1/00159.

References

- Wu W, Klockow JL, Zhang M, Lafortune F, Chang E, Jin L, et al. Glioblastoma multiforme (GBM): An overview of current therapies and mechanisms of resistance. *Pharmacol Res.* (2021) 171:105780. doi: 10.1016/j.phrs.2021.105780
- Dewdney B, Jenkins MR, Best SA, Freytag S, Prasad K, Holst J, et al. From signalling pathways to targeted therapies: unravelling glioblastoma's secrets and harnessing two decades of progress. *Signal Transduction Targeted Ther.* (2023) 8:400. doi: 10.1038/s41392-023-01637-8
- Migliorini D, Dietrich P-Y, Stupp R, Linette GP, Avery D, Posey J, June CH. CAR T-cell therapies in glioblastoma: A first look. *Clin Cancer Res.* (2018) 24:535–540. doi: 10.1158/1078-0432
- Eshhar Z, Waks T, Gross G, Schindler D. Specific activation and targeting of cytotoxic lymphocytes through chimeric single chains consisting of antibody-binding domains and the γ or ζ subunits of the immunoglobulin and T-cell receptors. *Proc Natl Acad Sci United States America.* (1993) 90:720–4. doi: 10.1073/pnas.90.2.720
- Wrona E, Potemski P. A novel immunotherapy — the history of CAR T-cell therapy. *Oncol Clin Pract.* (2019) 15:202–207. doi: 10.5603/OCP.2019.0016
- Kufel J, Lewandowski P. Terapia CAR-T w leczeniu guzów litych – zastosowanie i ograniczenia (in Polish) (Starowa Góra, Poland: Wydawnictwo Naukowe ArchaeGraph). (2023).
- Cohen AD, Garfall AL, Stadtmauer EA, Melenhorst JJ, Lacey SF, Lancaster E, et al. B cell maturation antigen-specific CAR T cells are clinically active in multiple myeloma. *J Clin Invest.* (2019) 129:2210–21. doi: 10.1172/JCI126397
- Pasvolosky O, Kebriaei P, Shah BD, Jabbour E, Jain N. Chimeric antigen receptor T-cell therapy for adult B-cell acute lymphoblastic leukemia: state-of-the-(C)ART and the road ahead. *Blood Adv.* (2023) 7:3350–60. doi: 10.1182/bloodadvances.2022009462
- Park JH, Rivière I, Gonen M, Wang X, Sénéchal B, Curran KJ, et al. Long-term follow-up of CD19 CAR therapy in acute lymphoblastic leukemia. *New Engl J Med.* (2018) 378:449–59. doi: 10.1056/NEJMoa1709919
- León-Triana O, Pérez-Martínez A, Ramírez-Orellana M, Pérez-García VM. Dual-target CAR-Ts with on- and off-tumour activity may override immune suppression in solid cancers: A mathematical proof of concept. *Cancers.* (2021) 13:703. doi: 10.3390/cancers13040703
- Bodnar M, Foryś U, Piotrowska MJ, Bodzioch M, Romero-Rosales JA, Belmonte-Beitia J. On the analysis of a mathematical model of CAR-T cell therapy for glioblastoma: Insights from a mathematical model. *Int J Appl Mathematics Comput Sci.* (2023) 33:379–94. doi: 10.34768/amcs-2023-002
- Bodnar M, Piotrowska MJ, Bodzioch M, Belmonte-Beitia J, Foryś U. Dual CAR-T cell therapy for glioblastoma: strategies to cure tumour diseases based on a mathematical model. *Nonlinear Dynamics.* (2025) 113:1637–66. doi: 10.1007/s11071-024-10258-x

Conflict of interest

The authors declare that the research was conducted in the absence of any commercial or financial relationships that could be construed as a potential conflict of interest.

The handling editor PM is currently organizing a Research Topic with the author UF.

Generative AI statement

The author(s) declare that Generative AI was used in the creation of this manuscript. The authors used ChatGPT (developed by OpenAI) exclusively for language editing and refinement. No content generation or intellectual contribution was provided by the tool. All scientific concepts, analyses, figures, and conclusions presented in this work are solely those of the authors.

Publisher's note

All claims expressed in this article are solely those of the authors and do not necessarily represent those of their affiliated organizations, or those of the publisher, the editors and the reviewers. Any product that may be evaluated in this article, or claim that may be made by its manufacturer, is not guaranteed or endorsed by the publisher.

Supplementary material

The Supplementary Material for this article can be found online at: <https://www.frontiersin.org/articles/10.3389/fimmu.2025.1563829/full#supplementary-material>

13. Szafrńska-Lęczycza M, Bodnar M, Piotrowska MJ, Krukowski M, Belmonte-Beitia J, Forys U. Influence of time delay on the dynamics of a mathematical model of CAR-T cell therapy with logistic tumor growth. *Discrete Continuous Dynamical Systems: Ser B.* (2025) 30(11):4498–515. doi: 10.3934/dcdsb.2025073
14. Scharovsky OG, Mainetti LE, Rozados VR. Metronomic chemotherapy: changing the paradigm that more is better. *Curr Oncol.* (2009) 16:7–15. doi: 10.1126/scitranslmed.aac5415
15. Bodnar M, Forys U. Three types of simple DDE's describing tumor growth. *J Biol Syst.* (2007) 15:453–71. doi: 10.1142/S0218339007002313
16. Szymańska Z, Skrzeczkowski J, Miasojedow B, Gwiazda P. Bayesian inference of a non-local proliferation model. *R Soc Open Sci.* (2021) 8:211279. doi: 10.1098/rsos.211279
17. Gwiazda P, Miasojedow B, Skrzeczkowski J, Szymańska Z. Convergence of the EBT method for a non-local model of cell proliferation with discontinuous interaction kernel. *IMA J Numerical Anal.* (2023) 43:590–626. doi: 10.1093/imanum/drab102
18. Elishmereni M, Kheifetz Y, Shukron I, Bevan G, Nandy D, McKenzie K, et al. Predicting time to castration resistance in hormone sensitive prostate cancer by a personalization algorithm based on a mechanistic model integrating patient data. *Prostate.* (2016) 7648–57. doi: 10.1002/pros.23099
19. Forys U, Nahshony A, Elishmereni M. Mathematical model of hormone sensitive prostate cancer treatment using leuprolide: A small step towards personalization. *PloS One.* (2022) 17:1–25. doi: 10.1371/journal.pone.0263648
20. Stein AM, Grupp SA, Levine JE, Laetsch TW, Pulsipher MA, Boyer MW, et al. Tisagenlecleucel model-based cellular kinetic analysis of chimeric antigen receptor-T cells. *CPT: Pharmacometrics Syst Pharmacol.* (2019) 8:285–295. doi: 10.1002/psp4.12388
21. Radunskaya A, Kim R, II TW. Mathematical modeling of tumor immune interactions: a closer look at the role of a pd-1 inhibitor in cancer immunotherapy. *Spora: A J Biomathematics.* (2018) 4, 41. doi: 10.30707/SPORA4.1Radunskaya
22. Ghorashian S, Kramer AM, Onuoha S, Wright G, Bartram J, Richardson R, et al. Tisagenlecleucel in adult relapsed or refractory diffuse large B-cell lymphoma. *Nat Med.* (2019) 25:1408–1414. doi: 10.1038/s41591-019-0549-5
23. Qi T, McGrath K, Ranganathan R, Dotti G, Cao Y. Cellular kinetics: A clinical and computational review of CAR-T cell pharmacology. *Advanced Drug Delivery Rev.* (2022) 188:114421. doi: 10.1016/j.addr.2022.114421
24. Haycock G, Schwartz G, Wisotsky D. Geometric method for measuring body surface area: A height-weight formula validated in infants, children and adults. *J Pediatr.* (1978) 93:68–6. doi: 10.1016/s0022-3476(78)80601-5
25. The MathWorks Inc. *MATLAB software version: 9.13.0 (r2022b)* (Natick, Massachusetts, United States). (2022).
26. Saltelli A, Tarantola S, Campolongo F, Ratto M. *Global sensitivity analysis for importance assessment.* John Wiley & Sons, Ltd (2002) p. 31–61. doi: 10.1002/0470870958.ch2
27. Qian G, Mahdi A. Sensitivity analysis methods in the biomedical sciences. *Math Biosci.* (2020) 323:108306. doi: 10.1016/j.mbs.2020.108306
28. Bogdańska MU, Bodnar M, Piotrowska MJ, Murek M, Schucht P, Beck J, et al. A mathematical model describes the Malignant transformation of low grade gliomas: Prognostic implications. *PloS One.* (2017) 12:1–24. doi: 10.1371/journal.pone.0179999
29. Swanson K, Harpold H, Peacock D, Rockne R, Pennington C, Kilbride L, et al. Velocity of radial expansion of contrast-enhancing gliomas and the effectiveness of radiotherapy in individual patients: a proof of principle. *Clin Oncol.* (2008) 20:301–8. doi: 10.1016/j.clon.2008.01.006
30. Woodward DE, Cook J, Tracqui P, Cruywagen G, Murray J, J.R. EA. A mathematical model of glioma growth: the effect of extent of surgical resection. *Cell Proliferation.* (1996) 29:269–88. doi: 10.1111/j.1365-2184.1996.tb01580.x
31. Kareva I, Waxman DJ, Lakka Klement G. Metronomic chemotherapy: an attractive alternative to maximum tolerated dose therapy that can activate anti-tumor immunity and minimize therapeutic resistance. *Cancer Lett.* (2015) 358:100–6. doi: 10.1016/j.canlet.2014.12.039
32. Ledzewicz U, Schättler H. Application of mathematical models to metronomic chemotherapy: What can be inferred from minimal parameterized models? *Cancer Lett.* (2017) 401:74–80. doi: 10.1016/j.canlet.2017.03.021
33. Bajger P, Bodzioch M, Forys U. Singularity of controls in a simple model of acquired chemotherapy resistance. *Discrete Continuous Dynamical Syst - B.* (2019) 24:2039–52. doi: 10.3934/dcdsb.2019083
34. Bajger P, Bodzioch M, Forys U. Numerical optimisation of chemotherapy dosage under antiangiogenic treatment in the presence of drug resistance. *Math Methods Appl Sci.* (2020) 43:10671–89. doi: 10.1002/mma.6958
35. Bodzioch M, Bajger P, Forys U. Angiogenesis and chemotherapy resistance: optimizing chemotherapy scheduling using mathematical modeling. *J Cancer Res Clin Oncol.* (2021) 147:2281–99. doi: 10.1007/s00432-021-03657-9
36. Kronik N, Kogan Y, Vainstein V, Agur Z. Improving alloreactive CTL immunotherapy for Malignant gliomas using a simulation model of their interactive dynamics. *Cancer Immunology Immunotherapy.* (2008) 57:425–39. doi: 10.1007/s00262-007-0387-z
37. Kogan Y, Forys U, Shukron O, Kronik N, Agur Z. Cellular immunotherapy for high grade gliomas: mathematical analysis deriving efficacious infusion rates based on patient requirements. *SIAM J Appl Mathematics.* (2010) 70:1953–76. doi: 10.1137/08073740X